3.2 THE INTERACTION OF INERTIAL DROPLETS WITH TURBULENCE AS A MECHANISM FOR ACCELERATED DROPLET SIZE SPECTRUM BROADENING: LABORATORY STUDIES OF PREFENTIAL CONCENTRATION, ENHANCED SETTLING AND TURBULENCE-INDUCED COLLISIONS OF SMALL INERTIAL DROPLETS

Colin P. Bateson*[1], Alberto Molina[1], Bogdan Rosa[2], Lian-Ping Wang[3] and Alberto Aliseda[1]
[1]University of Washington, Seattle, Washington
[2]Institute of Meteorology and Water Management, Poland
[3]University of Delaware

1. INTRODUCTION

Understanding rain formation processes and their effect on cloud temporal and spatial variability is an important focus of study in atmospheric science. Warm rain initiation (rain formation in the absence of ice crystals) involves three processes: condensation, collision-coalescence possibly due to turbulence, and collision-coalescence due to gravitational settling. The first and third processes are well understood and can be accurately modeled. But the importance of turbulent collision-coalescence on cloud droplet (20-60 μm in diameter) and intermediate droplet (60-200 μm in diameter) growth leading to precipitation is uncertain. Studies have shown that more accurate models of turbulent droplet collisions could explain some of the discrepancy between observed and predicted rates of precipitation formation.

Arenberg (1939) published the first study on the possible mechanisms by which turbulence could create droplet collisions, but advancements in our understanding of turbulence has made this work obsolete. Saffman and Turner (1956) understood that collisions are ultimately the result of non-zero relative velocities between objects. They suggested that there are two mechanisms by which turbulence can create relative velocity between cloud drops: (1) relative velocities arise due to spatial variations in the turbulent air motion, and (2) relative velocity can be created by variation in drop responses to turbulent motions owing to the drops' different inertia. Unlike Arenberg's results, these two statements still hold true today and as a result Saffman and Turner's work is considered the foundation upon which all further studies have built.

Woods, Drake, and Goldsmith (1972) were the first to experiment with the influence of turbulence on drop collisions by dropping collector drops vertically through a droplet-laden boundary layer flow developing on the top wall of a wind tunnel and measuring the resulting collision efficiency. The nature of their test setup limits their results to very specific flow conditions. De Almeida (1976, 1979) and Grover & Pruppacher (1985) studied changes in collision efficiency resulting from the interaction between droplets and turbulence but their results are limited by their simplifying assumptions for the droplet equations of motion. Maxey and Riley (1983) published the complete equation of motion for drops in turbulence, and Maxey went on to publish a series of computational studies (Maxey 1986, 1987a, 1987b) on inertial particles in increasingly complex representations of turbulent flow. Maxey's work shed much light on how heavy particles interact with carrier fluid turbulence; specifically, how the droplet's inertia causes them to move away from regions of high vorticity and concentrate in regions of high strain. Vaillancourt and Yau (2000) wrote a review of the work done to date on trying to quantify the cloud droplet collision problem. They summarized that while quantitative results were inconclusive and varied, collision efficiency is definitely a function of relative velocity and preferential drop concentration, and an increase in either results in an increase in collision efficiency. However, they noted that most studies failed to match the parameter space relevant to pre-precipitating cloud conditions.

More recently, the focus of research has shifted towards computational studies and DNS of the turbulent collision kernel and simulations of the collision process (Wang et. al. 2005, 2006; Pinsky et. al. 1999; Pinsky and Khain 2004; Pinsky et al. 2006). An accurate parameterization of the collision kernel could be used to quantify the importance of turbulence in droplet growth and rain formation, but the current body of computational work would benefit from experimental validation. The results presented in this paper can be used to validate and improve the computational work that has been done, or is currently in process.

* *Corresponding author address:* Colin P. Bateson, Univ. of Washington, Dept. of Mechanical Engineering, Seattle, WA 98195-2600; email: cbateson@uw.edu

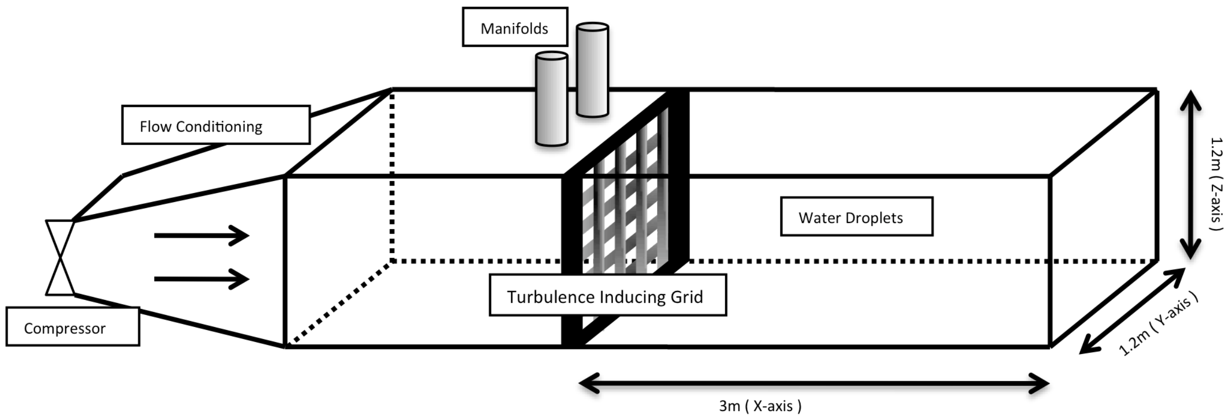

Figure 1: A diagram of the wind tunnel used for the experiments.

2. EXPERIMENTAL SETUP

2.1 Description

The experiments were conducted in a horizontal, blow-down style wind tunnel with a square test section measuring 1.2 m x 1.2 m and 3 m long. The two-stage, axial compressor moves air into a 2:1 expansion ratio section and then through a series of flow conditioning screens and honeycombs. The flow in the test section has a mean velocity of 1.4 m/s, and a Reynolds number of 10^5 based on the tunnel width. The turbulence intensity was measured to be about 30%, and the Reynolds number based on the Taylor microscale (Re_λ) was between 200 and 400.

Before entering the test section, the air passes through a biplane, turbulence-inducing grid. The grid is comprised of nine vertical and nine horizontal, hollow, aluminum tubes with diameter (d) equal to 2.54 cm and with a mesh spacing (M) of 10.16 cm. This results in a grid solidity ratio, $S = (d/M)(2 - d/M) = 0.44$, which puts the grid in the stable regime as defined by Baines and Peterson (1951). The Reynolds number based on the mesh size, $Re_M = U_\infty M/\nu$, is 10^4. Two-fluid atomizers embedded at the nodes of the evenly spaced grid introduce the water droplets into the flow. The flux of air from the high-speed gas jets in the atomizers makes the grid "active". The injection ratio (J), which is defined by Gad-el-Hak and Corrsin (1974) as the ratio of the jet flow rate (Q_j) to the total flow rate through the grid (Q_o), is small ($J = Q_j/Q_o \approx$ 1-2%). Their study showed that for a low injection ratio, such as the one used in our experiments, the jet flow will decrease the aerodynamic solidity of the grid and thereby render the flow downstream more stable and homogeneous.

The atomizers were constructed out of two brass tubes that were shaped and then brazed together so the high-momentum air jet impinges on the low-momentum water jet at a large angle, atomizing the liquid and producing a spray of small droplets. A photo of one of the atomizers is included as Figure 2. The atomizers were installed in the grid so the air jets exit parallel to the mean flow in the wind tunnel. The droplet size distribution and liquid mass fraction of the spray can be controlled by the air supply pressure and the water flow rate, as shown by Lazaro and Lasheras (1992).

The data for the experiments presented here were collected at atomizer flow rates of 3 liters per minute (LPM) of water and 50 standard cubic feet per minute (SCFM) of air, and a wind tunnel flow rate of approximately 2 m^3/s. This produced a volume fraction (α) of 2.5e-5 $m^3_{water}\ m^{-3}_{air}$ in the tunnel test section, which is equivalent to a liquid water content (LWC) of 25 g/m^3. This number is an order of magnitude higher than typical for cumulonimbus clouds. However, it is important to note that the mass loading of water is still low enough to assume that the turbulence is unaffected by the presence of the water droplets. The high LWC increases the probability of collisions during the short time the droplets have to interact inside the wind tunnel and facilitates the experimental characterization of the collision process. Therefore, these conditions allow us to study turbulent-induced droplet collisions and their effect on the overall process of warm rain formation in a controlled laboratory setting.

Figure 2: Photograph of one of the atomizers prior to its installation in the grid.

The Weber number for the droplets is of the order of 10^{-2}, therefore any deformation resulting from unsteady pressure forces in the flow field are quickly dominated by the restoring effects of surface tension.

For this reason it is safe to assume that the droplets remained spherical throughout the experiments.

Two pressure manifolds, for separate air and water supplies, were used to ensure the respective supply pressures were constant across all the atomizers. The manifolds were constructed out of aluminum pipe (5 in OD, 4 1/2 in ID) with closed covers connected to flanges welded on each end of the pipe. 81 holes were drilled and tapped in nine evenly spaced rows of nine holes equally distributed circumferentially around the manifolds. Barbed tube fittings were screwed into the holes in the manifold, and polyurethane tubing connected to the barbed tube fittings ran through holes cut into the wall of the wind tunnel and into the grid where they connected to the atomizers. Special care was taken to ensure that all the tubing running between the pressure manifolds and the atomizers is of the same length to equalize pressure losses.

In order to compensate for the hydrostatic pressure difference between the top and bottom of the grid, short lengths of microtubing were glued into the barbed tube fittings in the water manifold (Figure 3). A detailed calculation was done to determine the length of micro-tubing needed to induce losses in the water supply lines that would cancel the hydrostatic head resulting from the height difference between each row of fittings and its corresponding row of atomizers, thereby creating a uniform liquid flow rate in all the injectors. A diagram of the manifold-injector grid arrangement, including the height difference corresponding to the hydrostatic pressure difference, is shown in Figure 4. The microtube lengths were optimized for a range of water flow rates (0.8–6 LPM), so as to minimize the difference in flow rate between the top and bottom rows of atomizers for all the experiment flow conditions. Ultimately, the worst off-design condition resulted in a maximum difference in flow rate of 5% (at 0.8 LPM).

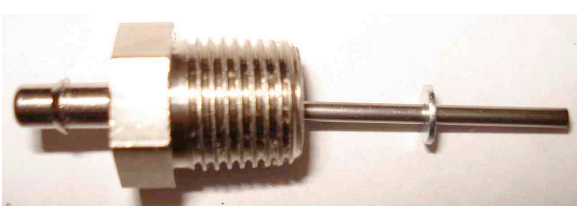

Figure 4: Photograph of a barbed tube fitting with a microtube installed.

Measurements to characterize the water droplets were made with a Phase Doppler Particle Analyzer (PDPA) system from TSI Inc. (Shoreview, MN.) By measuring the light scattered by a droplet passing through the intersection of two laser beams (a region called the "probe volume"), this system allows for non-intrusive, simultaneous measurements of the droplet's diameter, its time of arrival, and two components of its velocity. For this experiment, the receiver was positioned at an angle of 70 degrees to collect light in the first forward refraction mode. This has been shown to be the most effective for measuring water droplets in air. A thorough explanation of the measuring principle behind the PDPA system can be found elsewhere (Bachalo 1994).

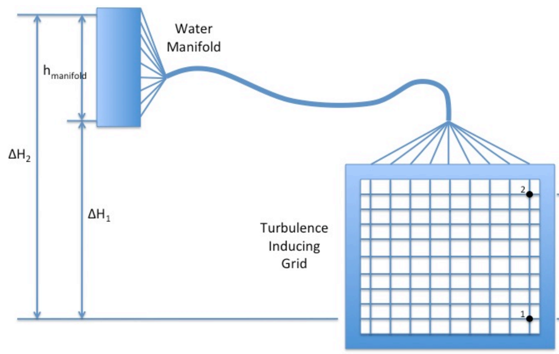

Figure 3: A diagram of how the hydrostatic pressure difference between the grid and the water manifold was measured.

Measurements were made at five stations along the length of the wind tunnel. (x = 0.654m, 1.44m, 1.71m, 2.19m and 2.94m). For this study, the grid is located at the origin, and the value of x describes the distance downstream from the grid. The exact locations were selected with the intent to distribute the measurement stations uniformly along the wind tunnel test section. Slight adjustments were made to avoid obstructions to the PDPA optical access caused by the wind tunnel support structure. To be consistent with the existing literature on grid turbulence, the measurement station locations were non-dimensionalized using the grid mesh spacing (M). In terms of M, PDPA measurements were made at the following five locations (x = 6.4M, 14M, 17M, 22M and 29M).

2.2 Characterization

In order to characterize the turbulent flow in the wind tunnel, and to verify that the turbulence was indeed isotropic and homogeneous, velocity data collected at each of the five measurement stations were used to calculate the statistics of the turbulence; namely, velocity average, root mean square (RMS) of the velocity fluctuations (u'), and the longitudinal one-dimensional energy spectrum (E_{11}).

In their research on grid-generated, homogeneous, isotropic turbulence, Comte-Bellot and Corrsin (1966) found that the inverse of the normalized turbulent kinetic energy $(U/u')^2$, when plotted as a function of distance down the wind tunnel, followed a power law. In their experiments, an exponent between 1.2 and 1.3 gave the best fit to their data. However, Wells and Stock (1983) proposed that in the "near region" for grid-generated turbulence, described as the region between 10M and 150M

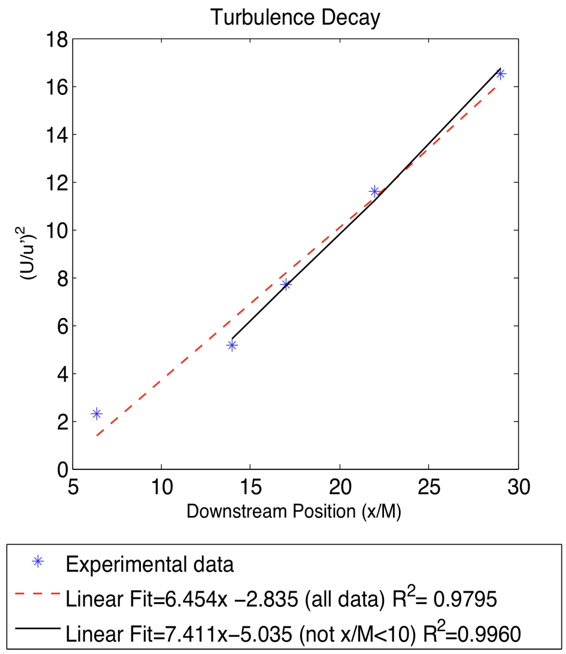

Figure 5: Turbulent intensity $(U/u')^2$ decay as a function of distance (x/M) downstream from the grid.

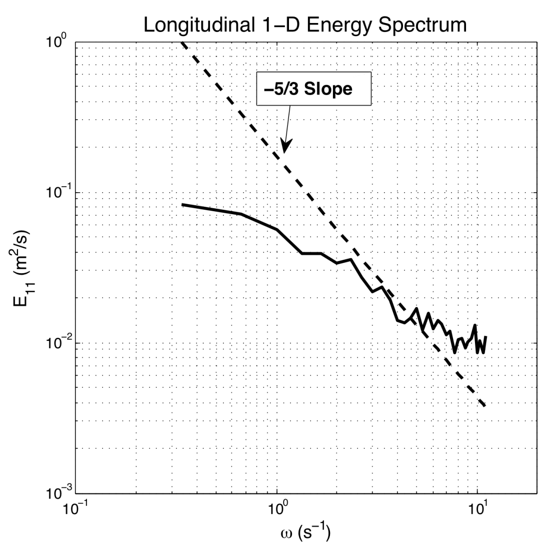

Figure 6: Longitudinal 1D turbulent energy spectrum at station 4 (x = 22M).

downstream from the grid, the turbulence intensity decay is inversely proportional to the distance downstream. Since all but one of the measurement stations for our experiment were within the near region, linear decay was expected. In the graph included as Figure 5, the values of $(U/u')^2$ for this experiment were plotted versus the distance from the grid. Two linear regressions to the data were made, one with all five data points, and a second that

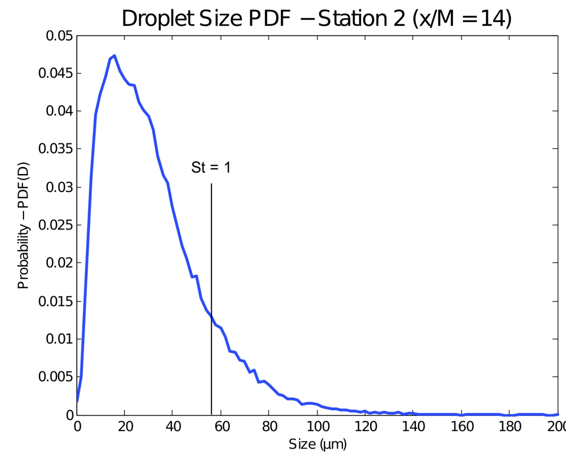

Figure 7: Probability distribution of droplet diameters measured at station 2. The black vertical line corresponds to the diameter of a droplet with Stokes number equal to 1.

excluded the data from the first station (x/M=6.4M, x=0.65m) since this point does not fit the definition of the "near region." The regression to the data from the last four measurement stations shows the decay fits the linear behaviour very well, which matches one of the characteristics of homogeneous and isotropic grid-turbulence.

The longitudinal one-dimensional turbulent energy spectrum (E_{11}) was calculated using the velocity measurements of the smallest droplets in our experiments based on the assumption that they have negligible inertia. Thus, they effectively behave as perfect flow tracers. Figure 6 shows E_{11} plotted as a function of frequency (ω) for station 2. A dashed line with a slope of -5/3 is included as a visual reference to the slope of the inertial range of turbulent energy spectra in Kolmogorov's theory. Unfortunately, the data rate from the PDPA was low, which not only placed an upper limit on the wave numbers we were able to resolve, but also raised the noise floor level at the largest wave number in the spectra measurements. Since the lack of precision precludes commenting on the evolution of the spectra across the measurement stations, and since all of the spectra were qualitatively similar, only one is presented here. More accurate characterization of the single-phase turbulence statistics, particularly at the smallest scales, is planned in the near future. This improved information will allow us to more accurately scale the droplet statistics and understand the dynamics. Qualitatively, though, we expect our analysis to stand.

Since the intent of this experiment was to relate our results to the evolution of cloud droplet size spectra, it was necessary to verify that the water droplets we created had an appropriate size distribution. Figure 7 is a plot of the probability density function of droplet diameter at station 2. Similar to the calculation of the turbulence decay, the data from

Table 1: A summary of the flow parameters

$Station$	x/M	$x\ (cm)$	$u'\ (cm/s)$	$\epsilon\ (cm^2/s^3)$	$\eta_k\ (\mu m)$	$\tau_k\ (ms)$	$u_k\ (cm/s)$	$\lambda\ (cm)$	Re_λ
1	6.4	65	100	12,300	235	3.55	6.61	-	-
2	14	144	59	1,690	385	9.58	4.02	0.98	373
3	17	171	56	1,260	415	11.1	3.74	0.88	318
4	22	219	46	950	445	12.8	3.48	0.85	252
5	29	294	41	780	467	14.1	3.32	0.87	230

station 1 were not included because the flow at that location was neither statistically stationary nor homogeneous. The plot in Figure 7 includes a line showing the diameter corresponding to a droplet with a Stokes number of 1. Since this diameter was well within the range of the droplet size spectrum, it shows that the droplets were significantly affected by the turbulence.

Real cloud droplet size spectra exhibit wide variation due to the large range of cloud conditions that occur in nature. Therefore, comparing our spectrum to a single real cloud droplet spectrum would be meaningless. However, it is worthwhile to note that our spectrum does exhibit the important general characteristics of a spectrum one would expect to see in a precipitating, or nearly precipitating cloud. For example, the majority of the droplets in this experiment have diameters under 60 microns – comparable to cloud droplets. Additionally, our spectrum has a tail of large diameter droplets that correspond to the few, "lucky", collector drops that are necessary for rain formation. This allows us to simultaneously study the collisions between two cloud droplets (< 60 μm) and the collisions between cloud droplets and collector-sized drops.

Important flow parameters and scales describing the conditions inside the wind tunnel are listed in Table 1. These include the turbulent dissipation rate (ε), the Kolmogorov length (η_k), time (τ_k), and velocity (u_k) scales, the Taylor microscale (λ), and the Reynolds number based on the Taylor microscale (Re_λ).

Taking the integral of the energy spectrum (Eqn. 1), we were able to get an approximate value for the turbulent kinetic energy dissipation rate (ε).

$$\varepsilon = 15\nu\int_0^\infty k^2 E_{11}(k)dk \tag{1}$$

This estimate of ε is limited in its accuracy by the lack of detailed information about the smallest scales in the turbulent kinetic energy spectrum referred to previously. For this reason we chose to calculate the Taylor microscale λ (used to characterize the turbulence through the Reynolds number Re_λ) using the integral length scale L_{11} (Eqn. 2) rather than ε.

$$\lambda/L_{11} = \sqrt{10/\mathrm{Re}_L} \tag{2}$$

From ε, the rest of the Kolmogorov microscales (Eqn 3, 4, and 5) can be calculated.

$$\eta = \left(\nu^3/\varepsilon\right)^{1/4} \tag{3}$$

$$\tau_\kappa = \left(\nu/\varepsilon\right)^{1/2} \tag{4}$$

$$u_\kappa = \left(\nu\varepsilon\right)^{1/4} \tag{5}$$

It is important to note that the goal of this experiment is to produce conditions where droplet collisions can be studied under the same physical environment as that present in clouds. In order to achieve this, we matched the Stokes number and the terminal velocity ratio of the droplets. The turbulence dissipation rate and droplet volume fraction are higher than the values found in cumulus clouds, but are still in a range where the physics are not influenced by these values (dilute flow with no turbulence attenuation by the droplets). The Reynolds number of the cloud would be impractical to reproduce in the laboratory, but the experiments are conducted at a high enough value that the results are characteristic of very high Reynolds number flow (asymptotic regime of Re).

While more work is still needed to completely characterize the flow conditions inside the wind tunnel, the initial measurements are encouraging as they indicate the turbulence is homogeneous and isotropic, and the important parameters match the conditions found in clouds during warm rain formation.

3. RESULTS

3.1 Radial Distribution Function

The preferential concentration of droplets was quantified using the radial distribution function (RDF). The RDF is a distribution function of the probability that two droplets, or a droplet pair, will be a certain distance apart. Originally derived for the field of solid mechanics to describe the distribution of atoms in crystalline or glassy structures, the RDF was first applied to multiphase fluid flows by Sundaram & Collins (1997) to characterize particle concentration. They showed that this statistic is important for quantifying the rate of collisions in a monodisperse droplet system. The rate of collisions is directly proportional to the RDF evaluated at the collision distance, which is the distance equal to the sum of the radii of the colliding drops.

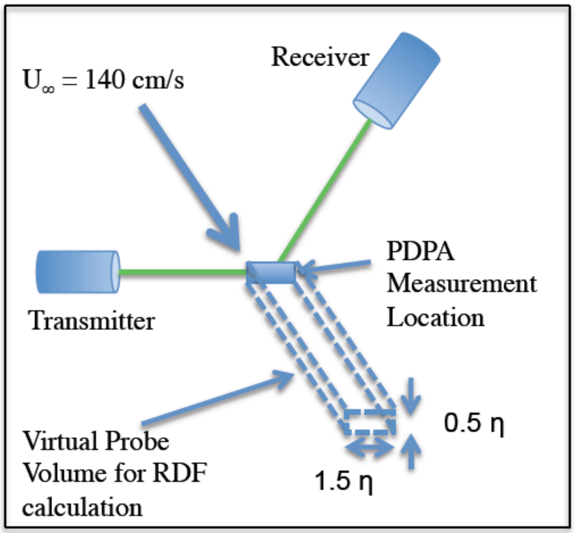

Figure 8: Diagram of the PDPA measurement location and probe volume.

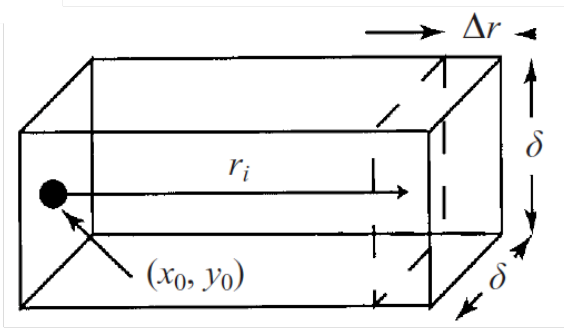

Figure 9: Diagram of how the finite size of the PDPA measurement point introduces error into the RDF. Figure taken from Holtzer & Collins (2004).

The RDF is a three-dimensional function, which is how it is applied in the formulation of the collision rate equation in Sundaram & Collins (1997). In our experiments, we compute a one-dimensional RDF from the PDPA measurements. Assuming the experiment is statistically stationary, and employing Taylor's hypothesis of "Frozen" turbulence (Taylor 1938), the temporal information on the droplet arrival at the probe volume can be converted to a position along a line oriented in the direction of the flow. From this position information, we construct probabilities of droplet pairs being separated by a certain distance, and the 1D RDF is the distribution of that probability.

The fact that the PDPA's probe has a finite cross section, and so the volume of fluid that passes through this cross section has a finite width, introduces a distortion in the RDF computed for very small separations (comparable to the width of the probe volume). A diagram showing this volume is included as Figure 8. The PDPA data does not contain any information on the sideways location of the particle when it crosses the probe volume and,

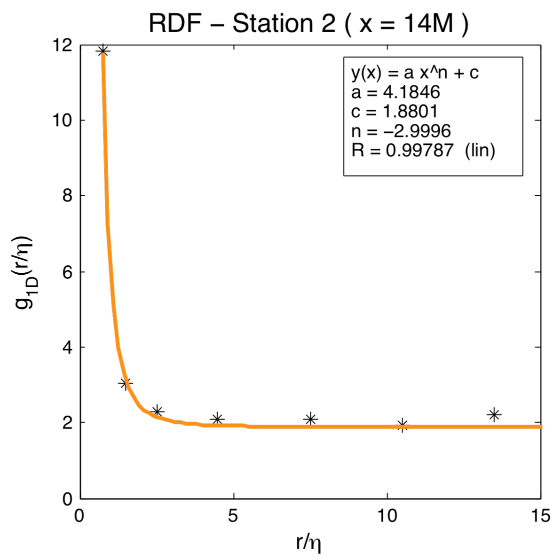

Figure 10: 1D radial distribution function at station 2. $g_{1D}(r/\eta)$, (*); Power law fit, (–).

therefore, the true separation distance between droplets may include some out-of-plane component. Referring to Figure 9, if the PDPA measures a droplet pair separation of r_i, the second particle could be anywhere in the volume δ by δ by Δr. This results in a true separation distance of r_i plus a component of δ. Ultimately the finite size of the PDPA measurement volume results in an underestimation of the true separation distance between particles. However, this error is only appreciable when r_i is the same order of magnitude as δ.

To circumvent this problem, the RDF data points were fit with a power law as suggested by Sundaram and Collins (1997). This allows the data to be extrapolated to very small separation distances on the order necessary to evaluate the RDF at the instant of collision. The RDF measured at station 2 in our experiment is plotted as a function of the separation distance normalized by the Kolmgorov length scale (Figure 10). The power law fit is plotted as a solid orange line. The RDFs at the three stations downstream from station 2 were all qualitatively very similar and so they are not included here.

3.2 Comparison to DNS results

The results of these experiments were used to validate direct numerical simulations (DNS) performed by Dr. Lian-Ping Wang's group at the University of Delaware. The DNS were run using either monodisperse droplet distributions with diameters of 10, 20, or 30 μm, or bidisperse droplet distributions with diameters of 10 and 20 μm, or 20 and 30 μm. Because our wind tunnel experiment creates a polydisperse diameter distribution, the differences in diameters were a source of discrepancy in the

Experiments ($\nu_{air} = 0.15\ cm^2/s$)						
x/M	t/T_e	$\epsilon\ (cm^2/s^3)$	u' (cm/s)	Re_λ	λ/η	u'/v_k
6.4	0	$1.23\ 10^4$	100	—	—	15.3
14	0.62	$1.69\ 10^3$	59	373	25.5	14.8
17	0.83	$1.26\ 10^3$	56	318	21.2	15.1
22	1.26	950	46	252	19.1	13.3
29	1.81	780	41	230	18.6	12.5

Simulations ($256^3\ DNS$, physical units)						
–	t/T_e	$\epsilon\ (cm^2/s^3)$	u' (cm/s)	Re_λ	λ/η	u'/v_k
–	0	400	15.5	120.3	21.6	5.40
–	0.4	360	14.0	96.6	19.3	4.99
–	0.8	230	11.7	78.3	17.4	4.49
–	1.2	170	9.8	69.6	16.3	4.22
–	1.6	110	8.4	62.3	15.5	4.01
–	2.0	70	7.2	57.5	14.9	3.86

comparisons. Additionally, exact matches between the turbulent flow parameters in the experiments and the DNS could not be made (Table 2), which is a second source of disagreement in the comparisons. Despite these two facts, the comparisons showed good qualitative agreement overall.

Figure 11 shows the comparison between droplet velocity RMS values for the DNS and the wind tunnel experiments. While the data sets do not agree perfectly due to the issues stated previously, they do exhibit a similar increasing trend with distance downstream and they have a similar order of magnitude.

Table 2: Turbulent flow parameters for wind tunnel experiments and DNS.

Figure 12 is a comparison between the RDF calculated from the experimental data collected at station 2 and six RDFs from the DNS calculated for a monodispersion of 20 μm droplets at six different eddy turn over times. Watching the flow evolve as it moves downstream in the wind tunnel experiments is analogous to increasing the eddy turn-over time in the DNS. In order to create a one-dimensional RDF similar to that calculated from the experimental results, the RDF for the 3D DNS results was calculated for a imaginary, long, slender volume with a 150 μm by 450 μm cross section. The experimental RDF was compared to that for a monodispersion of 20 μm droplets, which was the approximate value of the statistical mode in the experimental droplet diameter distribution. Again there is some discrepancy between the results for the experiments and the DNS, but the qualitative agreement is clear.

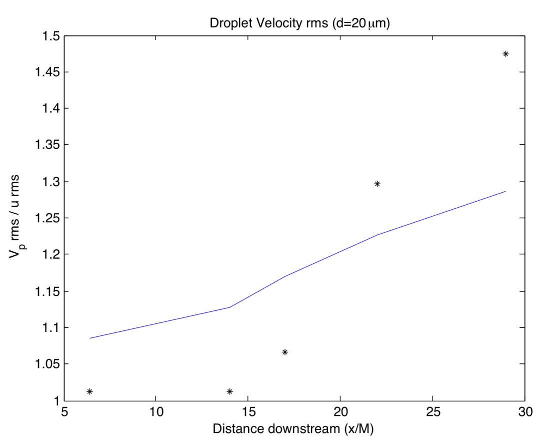

Figure 11: A comparison of droplet RMS values. The solid blue line represents the DNS values for a monodispersion of 20 micron droplets. The stars are data points from the wind tunnel experiments.

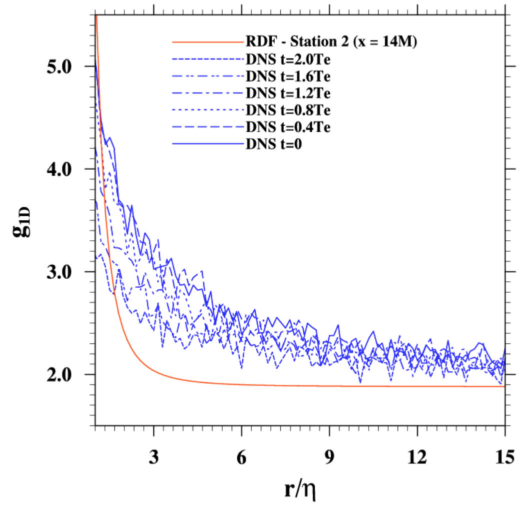

Figure 12: A comparison of the RDF calculated at station 2 for the wind tunnel experiments and the RDFs calculated from the DNS results for six different eddy turnover times.

As both the DNS and the experiments evolve towards more similar flow conditions, the RMS fluctuations and the RDFs presented here will show much better quantitative agreement.

4. CONCLUSION

The dynamics relevant to droplet collisions were studied using wind tunnel experiments. Water droplets were injected uniformly into slowly decaying, isotropic and homogeneous grid turbulence and a PDPA system was used to collect velocity, diameter, and arrival time data for the droplets. Using these data, the turbulence intensity decay, the 1D longitudinal kinetic energy spectrum, and the 1D RDF were computed for multiple locations downstream of the grid. The turbulence intensity was found to decay linearly with distance, which was the behavior expected for the near region in which our measurements were made. A low data collection rate limited the range of the energy spectra and as a result the smallest scales of the flow could not be resolved. The 1D RDFs for three different downstream locations were analyzed and the results showed evidence of significant preferential concentration. A simple power law provided good fits to the RDF data. These fits can be extrapolated to evaluate the RDF at separation distances relevant to collision processes. The 1D experimental RDFs were compared to 1D RDFs calculated from DNS of droplets in isotropic homogeneous turbulence. The experimental and DNS RDFs showed qualitative agreement. Exact matches were not expected due to small differences in the run parameters for the two sets of data.

Future work will focus on further characterization of the turbulence inside the wind tunnel. A high-speed camera will be used to collect two-dimensional PIV data from which one can calculate droplet preferential concentration and relative velocities. The later will be combined with visualizations of collision events to build statistics describing the coalescence efficiency of droplet collisions.

ACKNOWLEDGEMENTS

The authors would like to thank Marita Rodriguez for all her help constructing the experiment. Funding for this work was provided by the NSF through award ATM-0731248.

REFERENCES

Arenberg. D., 1939: Turbulence as the major factor in the growth of cloud drops. *Bull. Am. Meteorol. Soc.,* **20,** 444-448.

Bachalo, W. D., 1994: Experimental methods in multiphase flows. *Int. J. Multiphase Flow*, **20**, 261-295.

Baines, W.D., E.G. Peterson, 1951: An Investigation of Flow Through Screens. *Trans. Am. Soc. Mech. Eng,* **12,** 467-480.

Comte-Bellot, G., S. Corrsin, 1966: The use of a contraction to improve the isotropy of grid-generated turbulence. *J. Fluid Mech.* **25**, part 4, 657.

de Almeida, F.C., 1976: The collisional problem of cloud droplets moving in a turbulent environinent– Part I: A method of solution. *J. Atmospher. Sci.*, **33**, 1571-1578.

de Almeida, F. C., 1979: The collisional problem of cloud droplets moving in a turbulent environment–Part II: Turbulent collision efficiencies. *J. Atmospher. Sci.*, **36**, 1564-1576.

Gad-El-Hak, M., S. Corrsin, 1974: Measurements of the nearly isotropic turbulence behind a uniform jet grid. *J. Fluid Mech.*, **62**, part 1, 115-143.

Grover, S.N., H. R. Pruppacher, 1985: The effect of vertical turbulent fluctuations in the atmosphere on the collection of aerosol particles by cloud drops. *J. Atmospher. Sci.,* **42**, 2305–2318.

Holtzer G.L., L.R. Collins, 2002: Relationship between the intrinsic radial distribution function for an isotropic field of particles and lower-dimensional measurements. *J. Fluid Mech.*, **459,** 93-102.

Lázaro, B. J., J.C. Lasheras, 1992: Particle dispersion in the developing free shear layer. Part 1. Unforced flow. *J. Fluid Mech.*, **235,** 143–178.

Maxey, M.R., 1987a: The motion of small spherical particles in a cellular flow field. *Phys. Fluids*, **30**(4), 1915–1928.

Maxey, M.R., 1987b: The gravitational settling of aerosol particles in homogeneous turbulence and random flow fields. *J. Fluid Mech.*, **174,** 441–465.

Maxey, M.R., S. Corrsin, 1986: Gravitational settling of aerosol particles in randomly oriented cellular flows. *J. Atmospher. Sci.*, **43,** 1112–1134.

Maxey, M.R., J.J. Riley, 1983: Equation of motion for a small rigid sphere in a non-uniform flow. *Phys. Fluids,* **26**(4), 883–889.

Pinsky, M.B., A.P. Khain, M. Shapiro, 1999: Collisions of small drops in a turbulent flow. Part I: Collision efficiency problem formulation and preliminary results. *J. Atmospher. Sci.*, **56**(15), 2585–2600.

Pinsky, M.B., A.P. Khain, 2004: Collisions of small drops in a turbulent flow. Part II: Effects of flow accelerations. *J. Atmospher. Sci.*, **61**(15), 1926-1939.

Pinsky, M. B., A. P. Khain, B. Grits, M. Shapiro, 2006: Collisions of small drops in a turbulent flow. Part III: Relative droplet fluxes and swept volumes. *J. Atmospher. Sci.*, **63**, 2123-2139.

Saffman, P.G., J.S. Turner, 1956: On the collision of drops in turbulent clouds. *J. Fluid Mech.*, **1**, 16–30.

Sundaram, S., L.R. Collins, 1997: Collision statistics in an isotropic particle-laden turbulent suspension. Part 1. Direct numerical simulations. *J. Fluid Mech.*, **335**, 75–109.

Taylor, G.I., 1938: The spectrum of turbulence. *Proc. R. Soc. London, Ser. A,* **164** (919), 476-490.

Vaillancourt, P. A., M. K. Yau. 2000: Review of particle-turbulence interactions and consequences for cloud physics. *Bull. Am. Meteorol. Soc.*, **81**, 285–298.

Wang, L.P., O. Ayala, S.E. Kasprzak, and W.W. Grabowski, 2005: Theoretical formulation of collision rate and collision efficiency of hydrodynamically interacting cloud droplets in turbulent atmosphere. *J. Atmospher. Sci.*, **62**(7), 2433–2450.

Wang, L.P., Y. Xue, O. Ayala, W. Grabowski, 2006: Effects of stochastic coalescence and air turbulence on the size distribution of cloud droplets. *Atmos. Res.*, **82** (1-2), 416-432.

Wells, M.R., D.E. Stock, 1983: The effect of crossing trajectories on the dispersion of particles in a turbulent flow. *J. Fluid Mech.*, **136**, 31–62.